The photoreduction of selenite and selenate on the surface of a few layers black phosphorus and UiO-66 p-n junction heterostructure.

Kamogelo Martha Machabaphala,[a] Lerato Hlekelele [b] and Langelihle Nsikayezwe Dlamini [a*]

(S1)

XRD analyses

The d-spacing of the nanomaterials were calculated using Debye–Scherrer equation (**equation S1**) where D is the crystallite size, λ is the wavelength of X-ray (0.1541 nm) for CuKα, K = 0.89, θ is the diffraction angle and β is the full width at half maximum [1]. The d-spacing of the nanomaterials at 2θ is shown in **Table S1**. The d-spacing of UiO-66 on the heterostructure has increased indicating that little amount of FL-BP may be incorporated into the UiO-66 lattice.

$$D = \frac{K\lambda}{\beta \cos\theta} \qquad \textbf{(S1)}$$

Table S1: Intensity and d-spacing of photocatalysts at some 2θ values.

Photocatalysts	**2θ (°)**	**d-spacing (nm)**
Bulk BP	34.23	2.616
FL-BP	34.24	2.619
FL-BP on composite	34.24	2.617
UiO-66 on composite	7.40	11.94
UiO-66	7.42	11.89

(S2)

FTIR

FTIR was used to probe further into the structural properties of the nanomaterials that were shown to be UiO-66 and BP by PXRD. Here, the analyses were conducted mainly to elucidate the functional groups of the products. **Figure S1** shows the FTIR spectrum of UiO-66, BP, FL-

BP, and the FL/U(40) heterostructure. A strong absorption peak at 3422 cm^{-1} was observed on all the spectra indicating the presence of O-H which was attributed to absorbed water molecules on the surface of all the products.

The spectrum of UiO-66 showed a band at 1659 cm^{-1} representing C=O asymmetric stretch of DMF residing in the pores. The two intense bands at 1584 and 1395 cm^{-1} represent the O-C-O asymmetry and symmetry stretch vibrations, respectively, in the carboxylate groups of H_2BDC ligand [2], whereas, the small band around 1506 cm^{-1} represents the vibration of C=C of the benzene ring. At lower frequencies, the bands at 813, 749, 662 cm^{-1} are due to C=C stretch, O-H bend, and O-C-O bend of H_2BDC respectively. The band at 527 cm^{-1} belongs to the Zr-(OC) asymmetric stretch [3]. The bands observed were all matched with the expected functional groups of UiO-66 except for two bands which were attributed to molecules adsorbed onto the surface of the product.

The FTIR spectrum of FL-BP and bulk BP displayed stretching vibration around 1390 cm^{-1} ascribed to P-O bond. The bands at 1434 cm^{-1} to 1636 cm^{-1} are due to stretching vibration of P=O bond, the same results were reported by Song *et.al* [4]. This further demonstrates that the synthesis procedures yielded the anticipated products.

The FL/U(A) heterostructures showed bands of both FL-BP and UiO-66 indicating that UiO-66 was successfully incorporated on the surface of FL-BP. The transmittance of UiO-66 bands increased with an increase in loading of UiO-66 on FL-BP, and vice versa. The results observed here are in agreement with those observed from PXRD and Raman analyses.

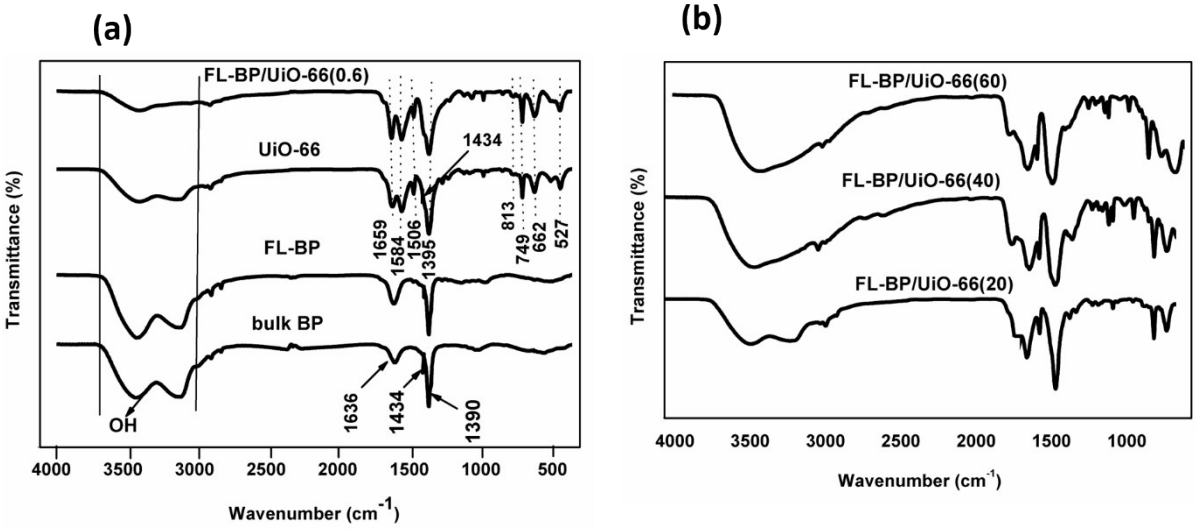

Figure S1. FTIR spectra of (a) UiO-66, bulk BP, FL-BP, and (b) FL/U(A) heterostructures.

(S3)

EDS

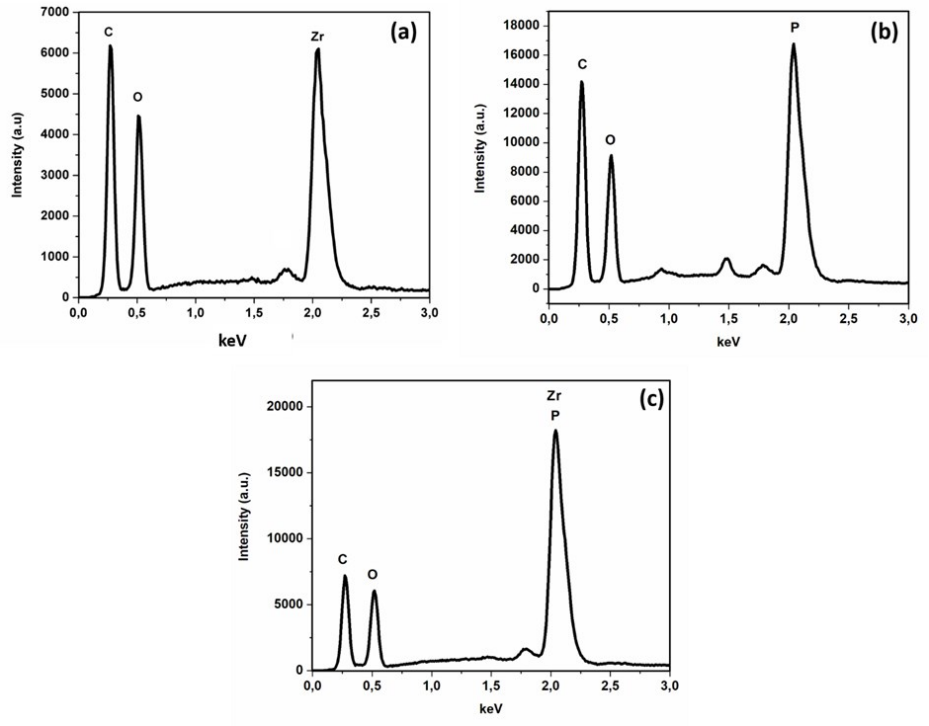

Figure S2. EDS spectrum of (a) UiO-66, (b) FL-BP and (c) FL/U(40).

(S4)

XPS

The valence states, surface elemental composition, and the formation of the nanomaterials were further investigated with XPS. **Figure S3a** shows the survey scan of the materials. The survey spectrum of UiO-66 indicates the presence of Zr, C, and O and that of FL-BP showed the presence of P, C, and O. On the other hand, the survey spectrum of the heterostructure FL/U(40) exhibited evidence that elements Zr, P, C, and O are indeed in the heterostructure, indicating that the heterostructure was composed of UiO-66 and FL-BP. The results obtained consistent with the observations made from EDX experiments.

High-resolution XPS spectra of Zr3d, P2p, C1s, and O1s were investigated. The presence of Zr is depicted (**Figure S3b**) at binding energy 181,6 and 184,0 eV representing $Zr3d_{5/2}$ and

$Zr3d_{3/2}$ respectively [5]. In **Figure S3c** peaks at 129.8 and 130.2 eV are due to $2p_{3/2}$, $2p_{1/2}$ respectively, showing the presence of BP [6].

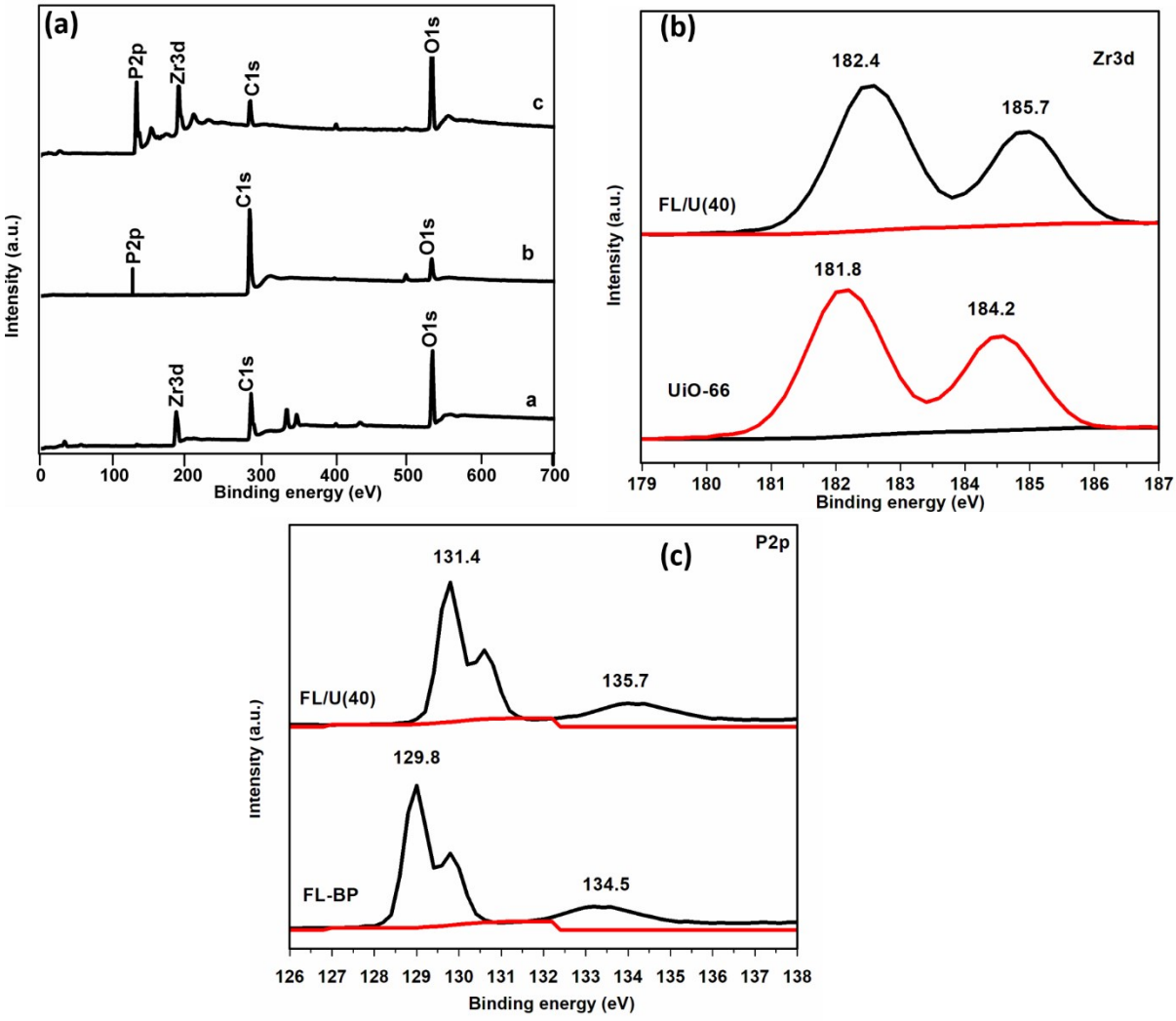

Figure S3: XPS spectra of UiO-66, FL-BP, and FL-BP/UiO(40) (a) Full scan, (b) Zr3d, and (c) P2p.

(S5)

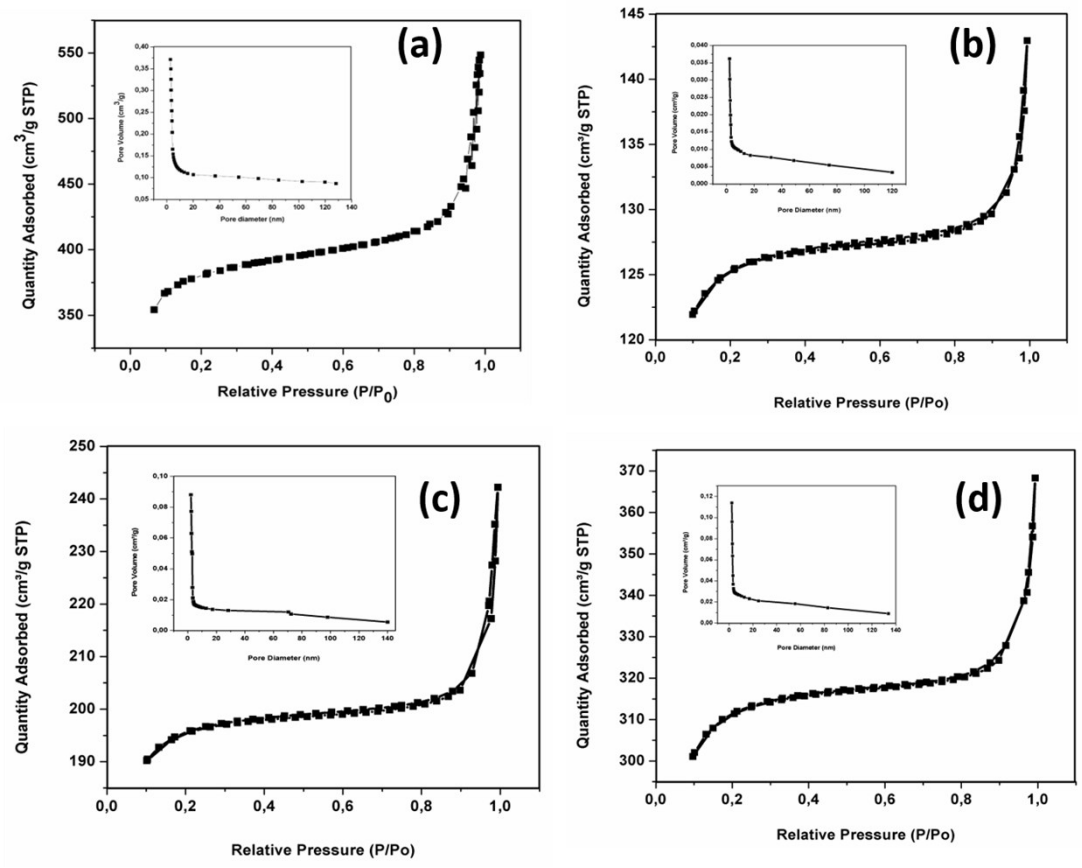

Figure S4: N_2 adsorption-desorption isotherm curve and pore size distribution curve (inset) of (a) UiO-66, (b) FL/U(20), (c) FL/U(40)and (d) FL/U(60).

(S6)

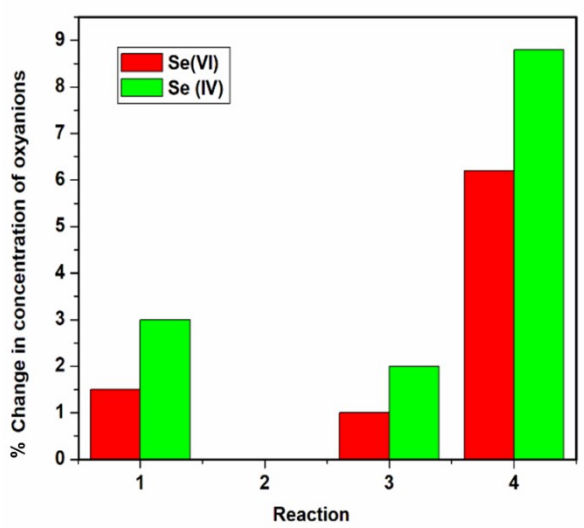

Figure S5: Change in concentration of oxyanions for reaction 1-4.

Pre-testing conditions optimization

(S7)

Photodegradation experiments conditions optimization

Effect of pH

The effect of pH on the photocatalytic reduction of selenate and selenite was studied as part of the efforts to draw out the conditions at which UiO-66 (the most basic photocatalyst synthesized in this work) works best. Photocatalytic reduction of Se oxyanions was studied at pH values of 1, 3, 5, 7,9, and 11. The plots are shown in **Figure S6.1a-b**. The results indicate that, in general, the reduction of selenate and selenite is more pronounced in more under acidic conditions. This is because UiO-66 is positively charged under acidic conditions as was shown in pzc studies and the selenium ions under investigation are negative. Photocatalytic reduction of selenate and selenite increased with an increase in pH to a maximum of 3 and 5 respectively. After the optimum pH, the photoreduction of the ions decreased with increasing pH. Under basic condition photoreduction of ions was poor, and there was insignificant photoreduction of selenium ions on pH of 11, Labaran and Vohra also observed insignificant photoreduction of selenate at a pH of 12.[7] On the other hand, chemically functionalizing UiO-66 with an amine group to form UiO-66-NH_2 as Wu *et al*.[8] did increased the point of zero charge from *ca*. pH=5.8 (reported in this work, **Fig. 10** in the manuscript) to *ca*. pH=8.0. Nevertheless, UiO-66-NH_2 as is the case in this work, UiO-66-NH_2 would also be positively charged at lower pH values thus photo-reduce negatively charged oxyanions better in acidic conditions.

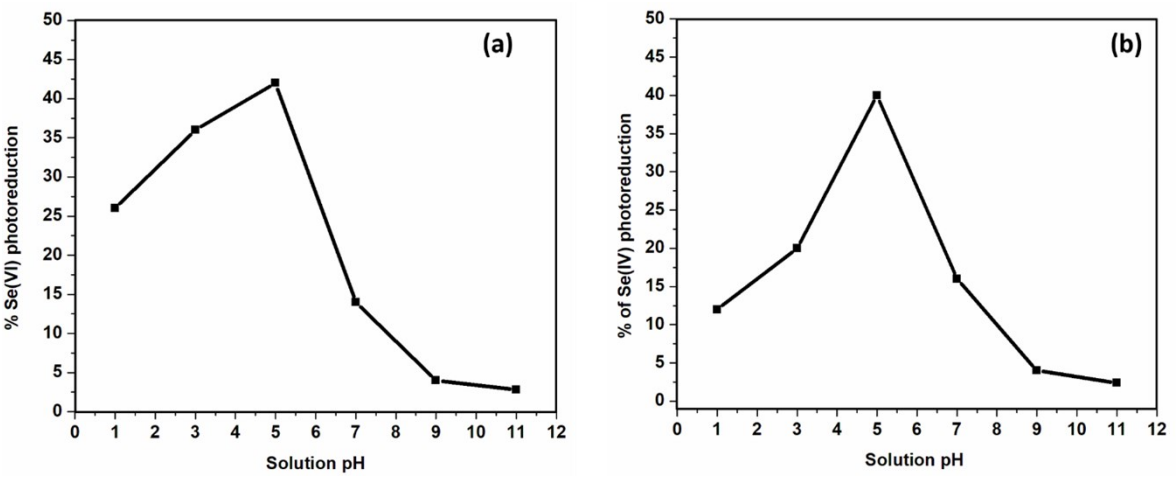

Figure S6.1: Effect of pH on photoreduction of 200 mL solution of 20 ppm (**a**) Se(VI) and (**b**) Se(VI) using 50 mg UiO-66, 60 ppm HCOOH for 1 hr.

Effect of catalyst loading

The optimization of the catalyst loading for the photoreduction of selenate and selenite was investigated to avoid the utilization of an excessive quantity of the photocatalyst. The results are shown in **Figure S6.2a-b**. The photocatalytic efficiency is influenced by the amount of photocatalyst hence it is very important to determine the optimum dose of the photocatalyst to achieve maximum reduction efficiency.

The photocatalytic reduction of both selenate and selenite increased with increasing UiO-66 (photocatalyst) loading until 30 mg, at which point the efficiency had begun to decrease with the increasing amount of the photocatalyst. The decrease in photocatalytic efficiency at high catalyst loading was because the high concentration of the photocatalyst particles caused turbidity. By definition, a turbid solution obstructs the transmittance of light thus some of the light was prevented light from reaching the surfaces of other photocatalyst particles. This consequently reduces the generation of active sites and, by extension, the reaction efficiency [9].

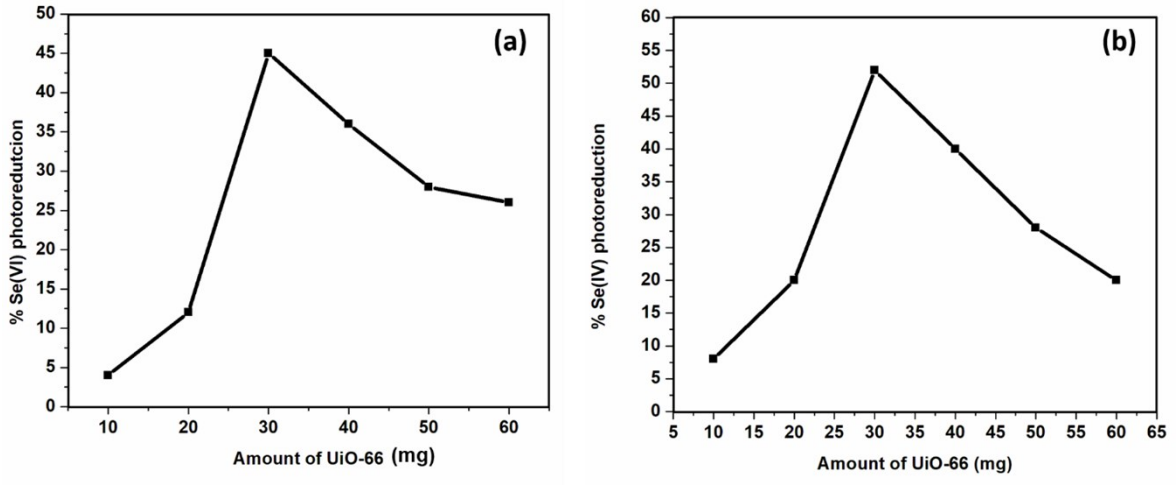

Figure S6.2: Effect of catalyst loading on photoreduction of 200 mL solution of 20 ppm (a) Se(VI) and (b) Se(IV) at pH = 3 for Se(VI) and 5 for Se(IV) using 60 ppm HCOOH for 1 hr.

Effect of selenium species concentration

The effect of the initial concentration of selenate and selenite ions on their removal using UiO-66 photocatalyst was investigated. The removal efficiency plots are shown in **Figure S6.3a-b.** The range investigated is 5-30 ppm. Here, it was observed that at concentration levels between 5 ppm and 15 ppm there was a linear increase at the efficiency UiO-66 photocatalyzed both selenate and selenite. This was attributed to that as the concentration of the pollutants was increased the likelihood that the species of the pollutants came into with the catalyst increased. This is especially true as these experiments were carried out in a short time. A steep decrease in the removal of the selenium ions was observed after their concentrations were increased beyond 15 ppm. This was ascribed to the high concentration of selenium ions in the solution blocks the light from falling on the UiO-66, leading to low photoreduction. The results show that 15 ppm was the optimum concentration for both selenate and selenite.

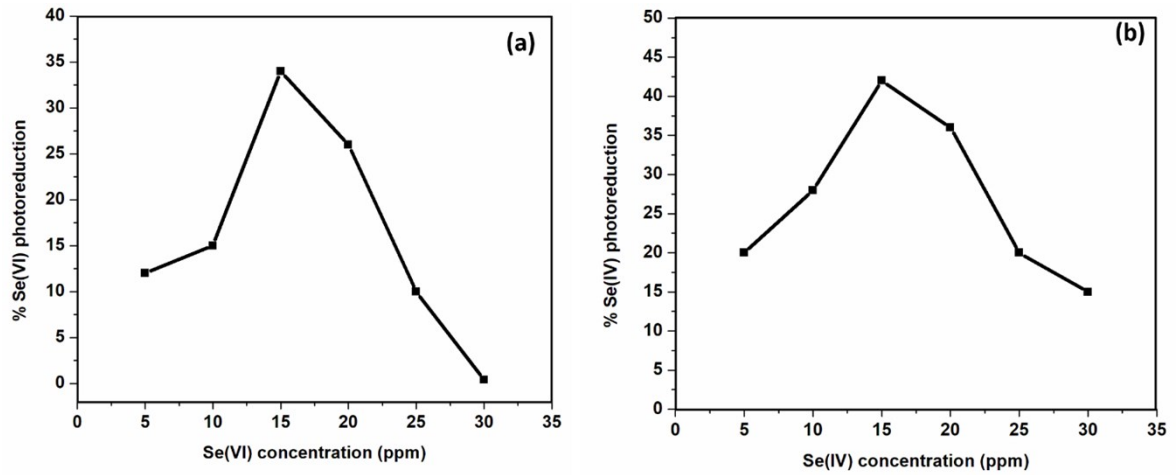

Figure S6.3: Effect of initial concentration of selenium ions on (a) Se(VI) and (b) Se(VI) photoreduced in a 200 mL solution at pH = 3 for Se(VI) and 5 Se(IV) using 30 mg UiO-66, 60 ppm HCOOH for 1 hr.

Effect of HCOOH concentration

The optimization of the amount of HCOOH used in the reduction of selenate and selenite using UiO-66 was also investigated (**Figure S6.4a-b**). This was done because HCOOH plays a significant role during the photoreduction of selenate and selenite. It serves as a hole scavenger functioning by trapping the holes generated in the VB when the photocatalyst is irradiated thus decreasing the recombination of electrons and holes. Formic acid is mostly used for photoreduction of selenate and selenite because its simple molecular structure of one carbon, makes its oxidation to carbon dioxide straightforward and there are fewer intermediate products and it readily adsorbs to surfaces under neutral and acidic conditions.[10] **Equation S2** shows the reaction between formic acid and positively charged valence band holes.

$$HCOOH \rightarrow CO_2 + 2H^+ + 2e^- \qquad \textbf{(S2)}$$

This is in the sense that at lower concentrations the photocatalytic activity of UiO-66 towards reducing selenate and selenite increased with increasing concentration of formic acid, reached an apex, and decreased (**Figure S6.4a-b**). The optimum concentrations of HCOOH for the reduction of selenate and selenite using UiO-66 were 75 and 50 ppmC respectively. The decrease in the photoreduction post the optimum concentration of formic acid was caused by the competition between HCOOH and Se ions on the surface of UiO-66. Also, it was seen that the optimum concentration of formic acid was different for the two selenium ions. This was attributed to that selenate has poor adsorption on UiO-66 [11]. This was also demonstrated by

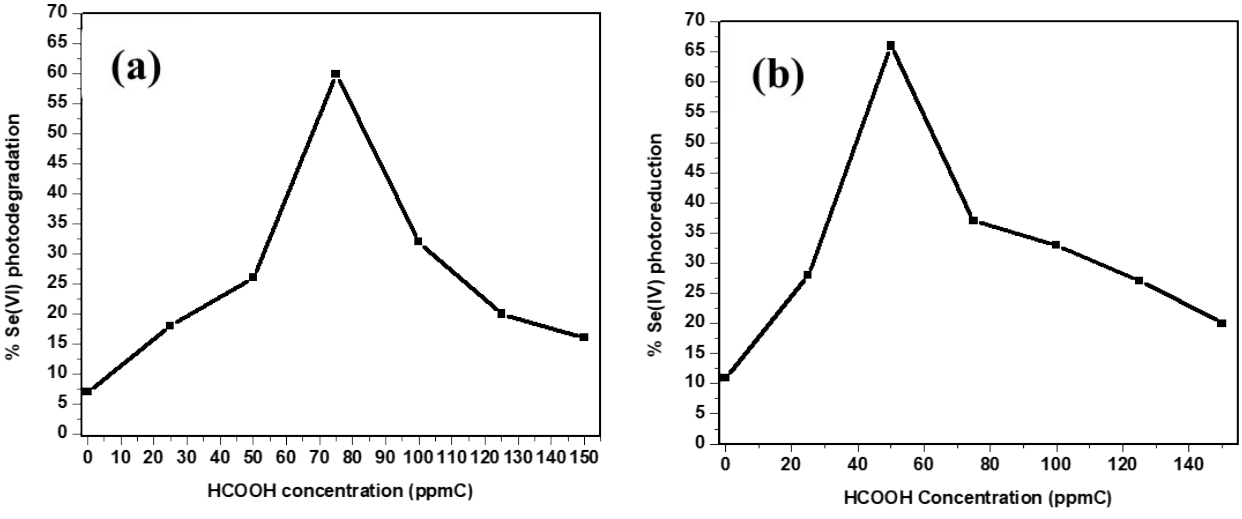

Nguyen *et.al* who reported that selenate demonstrated poorer adsorption onto TiO_2 photocatalyst relative to selenite in the presence of the same amount of formic acid [12].

Figure S6.4: Effect of HCOOH concentration towards reduction of 15 ppm (a) Se(VI) and (b) Se(IV) in a solution at pH = 3 for Se(VI) and 5 Se(IV) 30 mg UiO-66 for 1 hr.

(S8)

Table S2: Selenate reduction %, rate constants, and R^2 values.

Photocatalyst	k (min^{-1})	R^2	Reduction %
Bulk BP	0.01934	0.87284	69
FL-BP	0.02106	0.877655	72
FL/U(20)	0.02475	0.90484	78
FL/U(40)	0.03561	0.90835	89
FL/U(60)	0.02680	0.94058	81
UiO-66	0.01642	0.91744	60

Table S3: Selenite reduction %, rate constants, and R^2 values.

Photocatalyst	k (min^{-1})	R^2	Reduction %
Bulk BP	0.02229	0.87284	74

FL-BP	0.02455	0.87655	78
FL/U(20)	0.02634	0.96391	80
FL/U(40)	0.04624	0.94058	94
FL/U(60)	0.03364	0.90835	88
UiO-66	0.01719	0.91744	68

References

1 J. Cheng, W. Bao, D. Zhu, C. Tian, Q. Yin and M. Ding, *October*, 2009, **4**, 445–447.

2 Y. Cao, Y. Zhao, Z. Lv, F. Song and Q. Zhong, *J. Ind. Eng. Chem.*, 2015, **27**, 102–107.

3 Z. Guo, C. Xiao, R. V. Maligal-Ganesh, L. Zhou, T. W. Goh, X. Li, D. Tesfagaber, A. Thiel and W. Huang, *ACS Catal.*, 2014, **4**, 1340–1348.

4 S. Song, I. S. Raja, Y. Bin Lee, M. S. Kang, H. J. Seo and H. U. Lee, 2019, 1–7.

5 J. Ding, Z. Yang, C. He, X. Tong, Y. Li, X. Niu and H. Zhang, *J. Colloid Interface Sci.*, 2017, **497**, 126–133.

6 L. Wang, Q. Xu, J. Xu and J. Weng, *RSC Adv.*, 2016, **6**, 69033–69039.

7 B. A. Labaran and M. S. Vohra, *Environ. Technol. (United Kingdom)*, 2014, **35**, 1091–1100.

8 S. Wu, Y. Ge, Y. Wang, X. Chen, F. Li, H. Xuan and X. Li, *Environ. Technol.*, 2018, **39**, 1937–1948.

9 L. Hlekelele, P. J. Franklyn and S. H. Durbach, 2018, 4531–4542.

10 T. Tan, D. Beydoun and R. Amal, *J. Photochem. Photobiol. A Chem.*, 2003, **159**, 273–280.

11 J. Wei, W. Zhang, W. Pan, C. Li and W. Sun, *Environ. Sci. Nano*, 2018, **5**, 1441–1453.

12 V. N. H. Nguyen, D. Beydoun and R. Amal, *J. Photochem. Photobiol. A Chem.*, 2005, **171**, 113–120.